Earth and Planetary Science Letters 577 (2022) 117262

Contents lists available at ScienceDirect

Earth and Planetary Science Letters

www.elsevier.com/locate/epsl

New evidence for a long Rhaetian from a Panthalassan succession (Wrangell Mountains, Alaska) and regional differences in carbon cycle perturbations at the Triassic-Jurassic transition

A.H. Caruthers [a,*], S.M. Marroquín [b], D.R. Gröcke [c], M.L. Golding [d], M. Aberhan [e], T.R. Them II [f], Y.P. Veenma [g,p], J.D. Owens [h], C.A. McRoberts [i], R.M. Friedman [j], J.M. Trop [k], D. Szűcs [l], J. Pálfy [m,n], M. Rioux [o], J.P. Trabucho-Alexandre [g], B.C. Gill [b]

[a] Department of Geological and Environmental Sciences, Western Michigan University, Kalamazoo, MI 49006, USA
[b] Department of Geosciences, Virginia Tech, Blacksburg, VA 24061, USA
[c] Department of Earth Sciences, Durham University, South Road, Durham, County Durham, DH1 3LE, UK
[d] Geological Survey of Canada, Pacific Division, Vancouver, BC V6B 5J3, Canada
[e] Museum für Naturkunde Berlin, Leibniz Institute for Evolution and Biodiversity Science, 10115 Berlin, Invalidenstraße 43, Germany
[f] Department of Geology and Environmental Geosciences, College of Charleston, Charleston, SC 29424, USA
[g] Department of Earth Sciences, Universiteit Utrecht, P.O. Box 80115, 3508 TC Utrecht, the Netherlands
[h] Department of Earth, Ocean and Atmospheric Science, National High Magnetic Field Laboratory, Florida State University, Tallahassee, FL 32310-3706, USA
[i] Geology Department, State University of New York, Bowers Hall Rm 37, Cortland, NY 13045, USA
[j] Pacific Centre for Isotopic and Geochemical Research, University of British Columbia, Vancouver BC V6T 1Z4, Canada
[k] Department of Geology and Environmental Geosciences, Bucknell University, Lewisburg, PA 17837, USA
[l] Camborne School of Mines, University of Exeter, Penryn Campus, Cornwall, TR10 9FE, UK
[m] Department of Geology, Eötvös Loránd University, Pázmány Péter sétány 1/C, Budapest, H-1117, Hungary
[n] MTA-MTM-ELTE Research Group for Paleontology, Ludovika tér 2, Budapest, H-1083, Hungary
[o] Department of Earth Science, 1006 Webb Hall, University of California, Santa Barbara, CA 93106, USA
[p] Department of Earth Sciences, University of Cambridge, Downing Street, Cambridge, CB2 3EQ, UK

ARTICLE INFO

Article history:
Received 10 November 2020
Received in revised form 6 October 2021
Accepted 22 October 2021
Available online xxxx
Editor: T. Lyons

Keywords:
Norian-Rhaetian boundary
Triassic-Jurassic boundary
stable carbon isotopes
Wrangellia
Panthalassa
CAMP large igneous province

ABSTRACT

The end-Triassic mass extinction is one of the *big five* extinction events in Phanerozoic Earth history. It is linked with the emplacement of the Central Atlantic Magmatic Province and a host of interconnected environmental and climatic responses that caused profound deterioration of terrestrial and marine biospheres. Current understanding, however, is hampered by (i) a geographically limited set of localities and data; (ii) incomplete stratigraphic records caused by low relative sea-level in European sections during the Late Triassic and earliest Jurassic; and (iii) major discrepancies in the estimated duration of the latest Triassic Rhaetian that limit spatiotemporal evaluation of climatic and biotic responses locally and globally. Here, we investigate the Late Triassic–Early Jurassic time interval from a stratigraphically well-preserved sedimentary succession deposited in tropical oceanic Panthalassa. We present diverse new data from the lower McCarthy Formation exposed at Grotto Creek (Wrangell Mountains, southern Alaska), including ammonoid, bivalve, hydrozoan, and conodont biostratigraphy; organic carbon isotope ($\delta^{13}C_{org}$) stratigraphy; and CA-ID TIMS zircon U–Pb dates. These data are consistent with a Norian-Rhaetian Boundary (NRB) of ~209 Ma, providing new evidence to support a long duration of the Rhaetian. They also constrain the Triassic-Jurassic boundary (TJB) to a ~6 m interval in the section. Our TJB $\delta^{13}C_{org}$ record from Grotto Creek, in conjunction with previous data, demonstrates consistent features that not only appear correlative on a global scale but also shows local heterogeneities compared to some Tethyan records. Notably, smaller excursions within a large negative carbon isotope excursion [NCIE] known from Tethyan localities are absent in Panthalassan records. This new comparative isotopic record becomes useful for (i) distinguishing regional overprinting of the global signal; (ii) raising questions about the ubiquity of smaller-scale NCIEs across the TJB; and (iii) highlighting the largely unresolved regional vs. global scale of some presumed carbon cycle perturbations. These paleontological and geochemical data establish the Grotto Creek section as an important Upper Triassic to Lower Jurassic succession due to its

* Corresponding author.
E-mail address: andrew.caruthers@wmich.edu (A.H. Caruthers).

https://doi.org/10.1016/j.epsl.2021.117262

paleogeographic position and complete marine record. Our record represents the best documentation of the NRB and TJB intervals from Wrangellia, and likely the entire North American Cordillera.

1. Introduction

The Late Triassic to Early Jurassic was a dynamic interval of Earth history when the biosphere was severely disrupted by climatic and environmental changes that culminated in a major mass extinction (i.e., the end-Triassic mass extinction or ETE) across the Triassic-Jurassic Boundary (TJB; e.g., Alroy et al., 2008). It is considered one of the largest extinction events in Earth history and may be associated with rapid volcanogenic outgassing during the emplacement of the Central Atlantic Magmatic Province (CAMP; Fig. 1A; Wignall, 2001).

One of the most significant problems in understanding the timing of events around the ETE is the mass extinction itself. The removal of a large number of organisms from the global biosphere drastically decreased the number of taxa available for relative age assignments and, by consequence, our collective confidence in global stratigraphic correlation. The severity of climatic and environmental disruption at this time, however, significantly impacted global geochemical records, thus allowing alternative techniques (e.g., carbon isotope chemostratigraphy) to correlate strata and assign relative ages.

Considerable effort has been invested into identifying the global extent of biological turnover and environmental change during the latest Triassic and Early Jurassic using a diverse set of paleontological and geochemical data from the terrestrial and marine records (e.g., McElwain et al., 1999; Pálfy et al., 2000; Hesselbo et al., 2002; Whiteside et al., 2010; Schoene et al., 2010; Schaller et al., 2011; Steinthorsdottir et al., 2011). Detangling the local, regional, and global environmental signals from these datasets, however, remains an outstanding and important challenge that (given the available records) is exacerbated by (i) a geographically biased set of data, with the majority of published records from successions that represent deposition in the western part of the ancient Tethys Ocean and epeiric seaways (i.e., Europe, Fig. 1A); (ii) a low relative sea-level in the Tethys during the Late Triassic and earliest Jurassic which caused shallow-marine sites to be more susceptible to erosion and the development of significant hiatuses (e.g., Schoene et al., 2010); (iii) major discrepancies in current Late Triassic (Rhaetian) timescale models (e.g., Wotzlaw et al., 2014; Li et al., 2017). The latter has complicated the temporal correlation of geochemical datasets commonly used to interpret environmental change and the driving mechanisms of the ETE.

Here, we seek to address this gap by investigating the Upper Triassic to Lower Jurassic record from a well-preserved and largely unstudied sedimentary succession exposed in the Wrangellia terrane of North America (Fig. 1; Wrangell Mountains, USA). The Triassic to Jurassic rocks of this terrane accumulated in a tropical oceanic environment situated upon a subsiding oceanic plateau (e.g., Greene et al., 2010) in the Panthalassan Ocean. New data generated from the Grotto Creek section represent an important addition to existing end-Triassic records with implications toward a greater understanding of event timing and global carbon cycle perturbations.

2. Background

2.1. Trigger and driving mechanisms of the end-Triassic extinction

To date, both terrestrial and extraterrestrial causal mechanisms have been proposed for the ETE. As reviewed by Pálfy and Kocsis (2014) and Korte et al. (2019), the timing and magnitude of a bolide impact as the sole extinction mechanism lack significant evidence. The more widely accepted hypothesis links CAMP volcanism with a cascade of climatic and environmental feedbacks, which ultimately led to global mass extinction (e.g., Wignall, 2001; Carter and Hori, 2005; Korte et al., 2019) and is well supported by coeval peak extinction rates in siliceous (i.e., radiolarians) and calcifying organisms during the late Rhaetian (Kocsis et al., 2014). This hypothesis, known as the Volcanic Greenhouse Scenario or VGS (Wignall, 2001), has also been applied to explain several other mass extinctions linked to the emplacement of other large igneous provinces (e.g., Wignall, 2001).

The VGS proposes that perturbations to the global carbon cycle are one of the most ubiquitous underlying phenomena that accompany mass extinctions (e.g., Wignall, 2001). In this scenario, negative carbon isotope excursions (NCIEs) are caused by the input of ^{12}C-enriched carbon into the oceans and atmosphere by CO_2 from volcanic degassing, metamorphism of organic carbon-rich sediments by volcanic intrusions, and/or biogenic CH_4. Elevated atmospheric pCO_2 during the ETE is supported by stomatal index and paleosol data (McElwain et al., 1999; Schaller et al., 2011; Steinthorsdottir et al., 2011). Regardless of carbon source, all scenarios lead to atmospheric and oceanic warming and associated environmental feedbacks such as deoxygenation (and many others).

The organic carbon isotope ($\delta^{13}C_{org}$) records from the former Tethys Ocean and a handful of localities from Panthalassa show brief, large-amplitude NCIEs of ∼2–6‰ across coeval TJB successions (Ward et al., 2001; Guex et al., 2004; Hesselbo et al., 2002; Pálfy et al., 2007; Korte et al., 2019; and others). These records include what has been termed an *initial* NCIE before the TJB, which appears coeval with the main mass extinction interval (e.g., Korte et al., 2019). In many records, the *initial* NCIE is followed by a transient increase in $\delta^{13}C_{org}$ and then a second or *main* NCIE that extends well into the early Hettangian (e.g., Korte et al., 2019). Similar general trends have also been observed in the $\delta^{13}C$ of fossil wood (Hesselbo et al., 2002) and compound-specific $\delta^{13}C$ (e.g., Whiteside et al., 2010; Williford et al., 2014) at several locations, supporting their global nature.

Counter to this interpretation, some $\delta^{13}C_{org}$ records lack two clear NCIEs from the TJB interval (Pálfy et al., 2007), and other potentially correlatable NCIEs are identified in the uppermost Triassic at some European locations with varied interpretations for their correlation (e.g., Lindström et al., 2017). Whether these NCIEs recorded from Tethyan successions exist in Panthalassa remains outstanding (e.g., Du et al., 2020). Until more data are generated that may resolve these smaller NCIEs (e.g., Heimdal et al., 2020), there is insufficient evidence to support a global driver for their occurrence.

2.2. The Triassic-Jurassic boundary interval

Although the Kuhjoch section in Austria was ratified as the GSSP for the base of the Jurassic (Hillebrandt et al., 2013), the choice of this section has drawn criticism (e.g., Palotai et al., 2017). The formal base of the Jurassic is defined by the lowest occurrence of *Psiloceras spelae tirolicum* (Hillebrandt et al., 2013) and several other variably utilized stratigraphic markers which typically include a combination of paleontological and geochemical data. For example, carbon isotope stratigraphy has been utilized

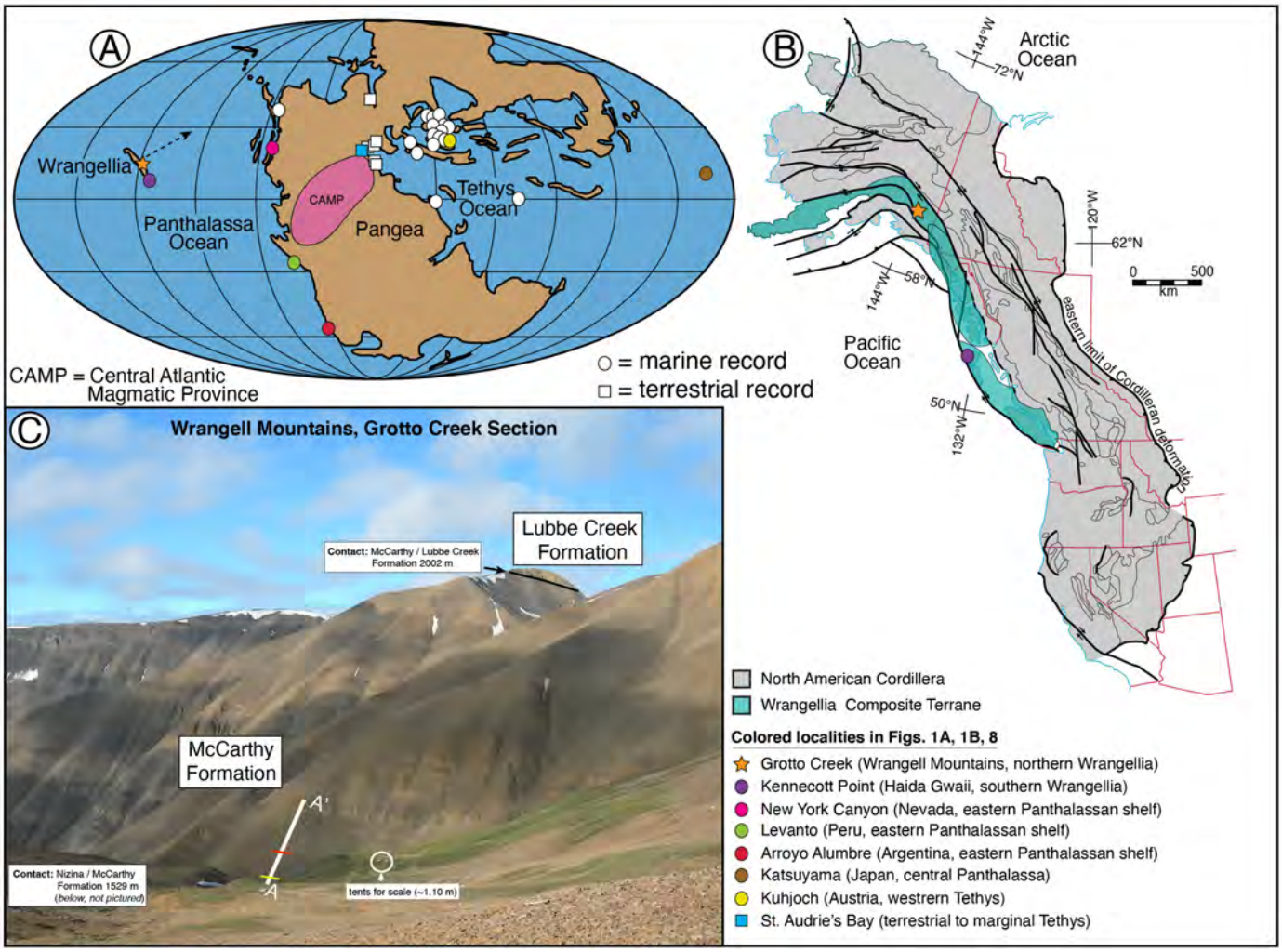

Fig. 1. A. Global Late Triassic paleogeographic reconstruction showing the approximated location of the Central Atlantic Magmatic Province (CAMP) at the TJB, the allochthonous terrane Wrangellia, and relevant coeval marine and terrestrial records (base map after Blakey, 2014; data localities after Hesselbo et al., 2002; Whiteside et al., 2010; Schoene et al., 2010; Williford et al., 2014 and references therein). Dashed arrow indicates hypothetical direction of future tectonic displacement of northern Wrangellia. **B.** Present-day tectonic map of western North America showing location of the Wrangellia composite terrane, the Wrangell Mountains, and Haida Gwaii (modified from Colpron and Nelson, 2009). **C.** Photograph of the Grotto Creek section showing the relevant stratigraphy, approximate location of measured section (A–A′; base is below ridge in foreground at 61°30′13.23″N, 142°26′31.51″W), and positions of the Norian-Rhaetian boundary (yellow line) and Triassic-Jurassic boundary (red line).

with the TJB demarcated between the initial and main NCIEs (e.g., Hesselbo et al., 2002; Korte et al., 2019). In terms of paleontological markers, the TJB is defined by the disappearance and/or appearance datums of organisms in three taxonomic groups (see Fig. 2): (i) ammonoids, lowest occurrence of *Psiloceras spelae* and *P. tilmanni* above species of *Rhabdoceras*, *Placites*, *Arcestes*, *Vandaites*, *Cycloceltites* and *Megaphyllites*; (ii) conodonts, the total extinction of the class; and (iii) radiolarians, by the disappearance of *Betraccium*, *Risella*, *Globolaxtorum tozeri*, *Livarella valida*, and *Pseudohagiastrum giganteum*, and the appearance of low-diversity spumellarians along with genera *Charlottea*, *Udalia*, and *Parahsuum* s.l. (Carter and Hori, 2005). Radiolarians represent a prominent example showing a temporal relationship between the onset of CAMP volcanism (as marked by geochemical anomalies) and rapid species-level turnover at the ETE / TJB transition (Carter and Hori, 2005; Kocsis et al., 2014).

Although *Aegerchlamys boellingi* was previously suggested as a marker for the basal Hettangian (e.g., McRoberts et al., 2007), recent correlations of the lower Fernie Formation at Williston Lake, British Columbia Canada (Larina et al., 2019) confirm several levels bearing *Aegerchlamys boellingi* (McRoberts unpublished collections) above the last occurrence of *Monotis subcircularis*. Also concerning the extinction of Class Conodonta at the TJB, reports indicate that *Neohindeodella detrei* occurs in the lowermost Hettangian overlapping with *Psiloceras* and Jurassic radiolarians in Csővár, Hungary (Pálfy et al., 2007; Du et al., 2020). Having additional data with which to assess and/or reinforce these stratigraphic relationships with other Rhaetian fauna is imperative for an improved understanding of the TJB interval and the ETE.

Absolute calibration of the latest Triassic to TJB interval has been the subject of numerous contributions (e.g., Pálfy et al., 2000; Guex et al., 2012) using a wide variety of radiometric dating techniques in terrestrial and marine sedimentary sequences, but with variable results. Recent U–Pb TIMS dating of two ash layers between the last occurrence of *Choristoceras* and the first occurrence of *Psiloceras* within a TJB section from Peru yielded single-grain U–Pb zircon dates of 201.51 ± 0.15 and 201.39 ± 0.14 Ma (Schoene et al., 2010; Guex et al., 2012; recalculated by Wotzlaw et al., 2014 based on revised tracer calibration). These recalculated dates provide robust age constraints on the TJB.

In addition, magnetostratigraphic and cyclostratigraphic analyses have been applied in an attempt to provide higher-resolution absolute age constraint(s) on this interval (e.g., Kent et al., 2017; Li et al., 2017; Galbrun et al., 2020). Most prominently, data from the

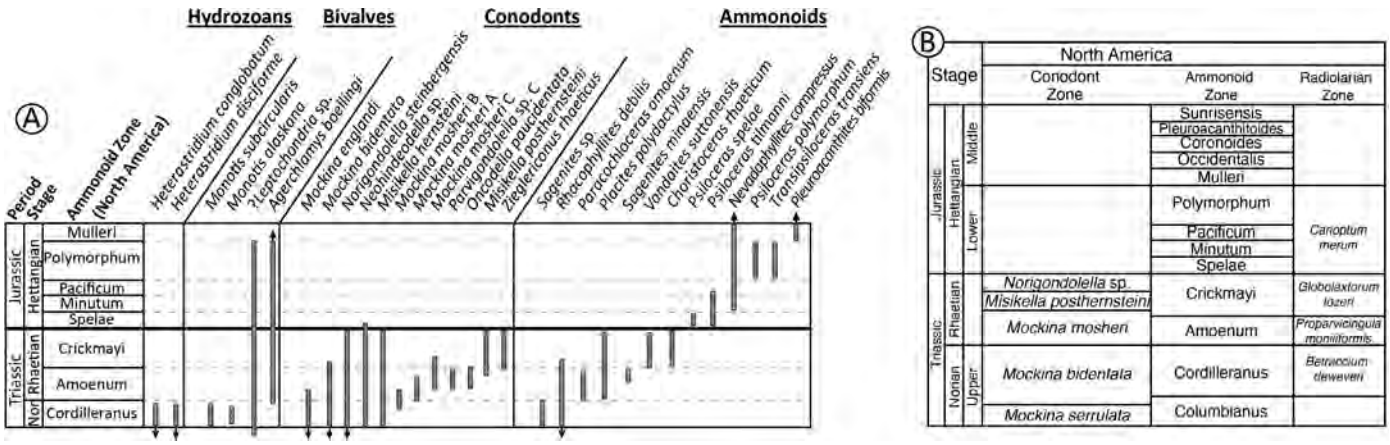

Fig. 2. Taxonomic range chart and zonal schemes for selected Late Triassic to Early Jurassic faunas of North America. **A.** Hydrozoans (after Senowbari-Daryan and Link, 2019), bivalves (after McRoberts et al., 2007) conodonts (Rigo et al., 2018 and others); ammonoids (after Tozer, 1994; Taylor et al., 2001; Guex et al., 2004; Longridge et al., 2007, 2008). **B.** Relevant conodont, ammonoid and radiolarian zones of North America (after Rigo et al., 2018 and references therein). *Note:* Nor = Norian; Ammonoid zonations used herein denote a zone name with reference to an assemblage of taxonomic ranges, rather than the range of a particular species.

fluvial-lacustrine succession in the Newark Basin have been used to develop a Newark astrochronostratigraphic polarity timescale (or Newark APTS; e.g., Kent et al., 2017). While correlations of some marine successions to the Newark APTS have been proposed (e.g., Maron et al., 2019), most studies of marine successions rely on a combination of biostratigraphic and chemostratigraphic data for temporal constraint and correlation.

2.3. A short vs. long Rhaetian

In contrast to the TJB, there is no consensus on the age of the Norian-Rhaetian Boundary (NRB) and the duration of the Rhaetian (i.e., the youngest age of the Late Triassic). At present, there are divergent age models based on a combination of biostratigraphic, geochemical, and magnetostratigraphic datasets and astrochronologic models that suggest conflicting durations (e.g., Wotzlaw et al., 2014; Golding et al., 2016; Li et al., 2017; Kent et al., 2017; Rigo et al., 2020; Galbrun et al., 2020). Models suggest either a *short* or *long* Rhaetian where the lower boundary with the Norian is constrained at 205.7 or 209.5 Ma, respectively, corresponding to a total duration (of the Rhaetian) that could have lasted approximately 4 to 8 Ma (see Li et al., 2017).

The currently accepted definition of the NRB in marine successions is the first appearance of the conodont *Misikella posthernsteini* (Krystyn, 2010). There is, however, disagreement regarding at what point this species can be considered a distinct taxon from its predecessor *Misikella hernsteini* (e.g., Galbrun et al., 2020), a problem exacerbated by recognition of two distinct morphotypes of *M. posthernsteini*. By using the first occurrence of *M. posthernsteini* in a broader sense (*sensu lato, s.l.*), as in the Steinbergkogel Section near Hallstatt, Austria, the NRB occurs just above a change from a normal to a reverse polarity magnetozone in the 207–210 Ma interval, suggesting a *long* ∼8–9 Ma Rhaetian (Krystyn et al., 2007; Muttoni et al., 2010; Li et al., 2017). By using the first occurrence of a more developed form (i.e., *sensu stricto, s.s.*), the duration becomes much shorter (Rigo et al., 2016; Wotzlaw et al., 2014). The *s.s.* case is proposed as the marker for the base of the Rhaetian at the Pignola-Abriola section in Italy, where the NRB is very high within a reversed polarity magnetozone (viz., 205.7 Ma), suggesting a ∼4 Ma duration (Maron et al., 2015; Kent et al., 2017). An additional problem is the rare occurrence of *M. posthernsteini* (both *s.l.* and *s.s.*) outside the Tethys region, which hampers their use for global correlation.

Interestingly, interpretations from the terrestrial Newark Supergroup (eastern North America) and the astrochronology and geomagnetic polarity timescale (APTS) derived from it have been used to support both *short* and *long* durations for the Rhaetian. Correlations of marine strata to the Newark APTS 2017 (Kent et al., 2017) indicate that the NRB may occur in either the E17 chron (near the *normal* to *reverse* polarity flip, at ∼209.5 Ma) or the E20 chron (*reversed* polarity at ∼206–205 Ma) (as summarized by Li et al., 2017, Fig. 1). A short duration for the Rhaetian requires a ∼2–5 Ma hiatus in Newark-APTS (Newark Gap; Tanner and Lucas, 2015), but whether such a hiatus exists remains highly contentious (e.g., Kent et al., 2017). These discrepancies in the age models for the Rhaetian help reinforce the importance and need for more studies with diverse sets of chronological data focused on the temporal correlation of this critical interval of time.

Data presented here from an oceanic Panthalassan locality with abundant fossils and radioisotopically datable bentonite beds crucially offer a new opportunity to assess the timing and duration of the NRB and TJB intervals in a conformable succession with a complete record of those intervals. This is critical for refining timescale calibration and assessing the global timing of carbon cycle perturbations and biotic crises during the ETE.

3. Geological setting

The Triassic to Lower Jurassic portion of the Wrangellia terrane is conformable and rests nonconformably on a thick succession of flood basalts in the Western Cordillera of North America (Greene et al., 2010). The terrane contains several tectonostratigraphic units across nearly 2000 km throughout westernmost British Columbia and Alaska (Fig. 1B). The type section, or northern block, is located in the Wrangell Mountains of southcentral Alaska, whereas the southern block is best documented on Vancouver Island and Haida Gwaii in western British Columbia, Canada. Although its position in Panthalassa and accretionary history have been debated, paleomagnetic, geochronologic, and paleontologic datasets indicate that Wrangellia was located at tropical latitudes in eastern Panthalassa during the Late Triassic (e.g., Caruthers and Stanley, 2008) before colliding with the continental margin of North America during the Middle Jurassic (southern block) and Cretaceous (northern block; e.g., Trop et al., 2020).

The Upper Triassic portion of Wrangellia represents an extensive carbonate platform and reef system inhabited by abundant and locally diverse marine biota (e.g., Caruthers and Stanley, 2008). In the Wrangell Mountains this section is represented by two calcareous units: the supratidal/intertidal to shallow subtidal, thick- to very thick-bedded Chitistone Formation and the deeper water,

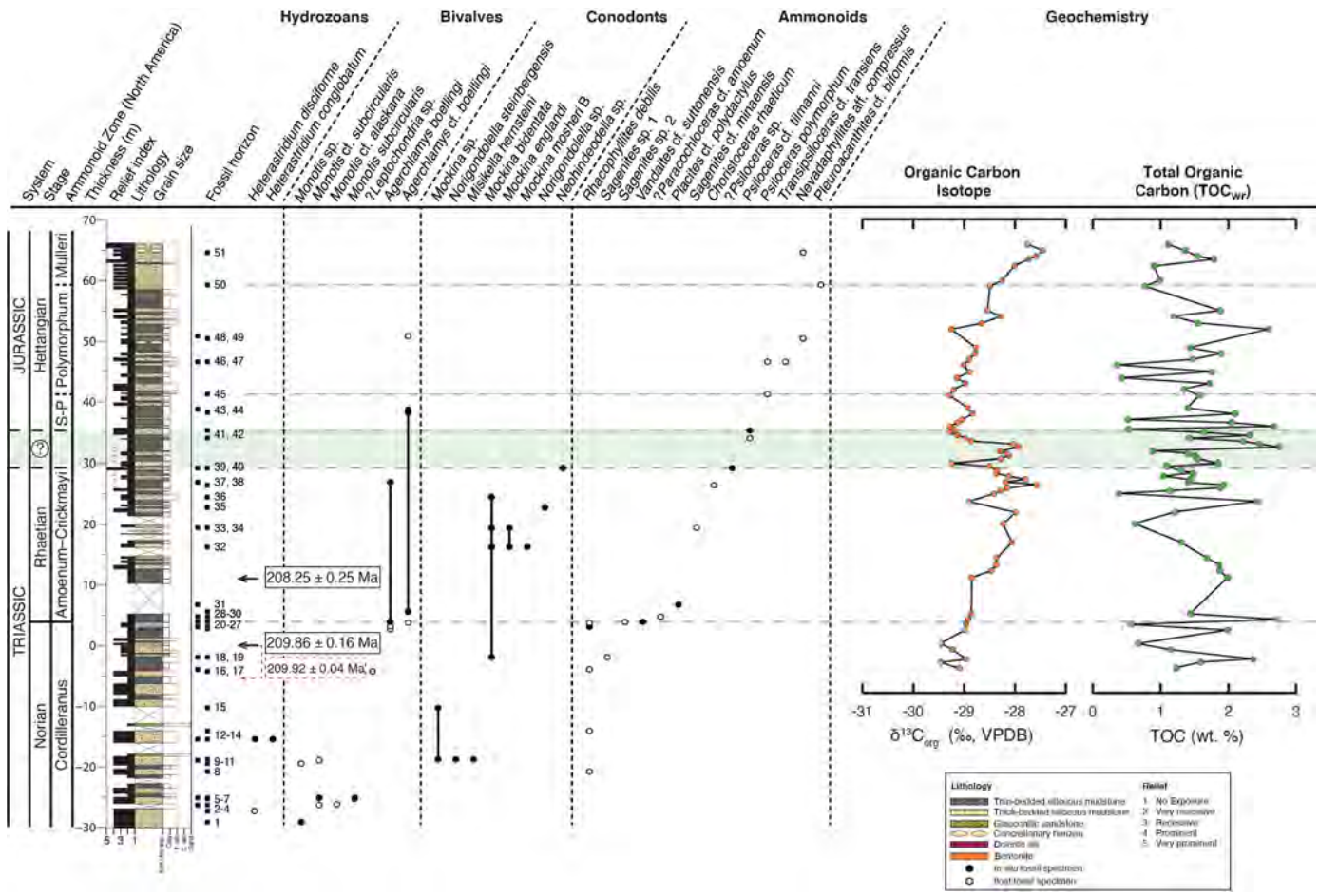

Fig. 3. Compilation data from the Grotto Creek section, Alaska (base at 61°30′13.23″N, 142°26′31.51″W) showing combined lithological, paleontological, and geochemical results. *Note*: Shaded area represents the suspected TJB interval; vertical hash marks indicate intervals of poor exposure; Dashed red box and corresponding dashed red arrows represent suspected interval of dated ash by Witmer (2007), solid black arrows and boxes denote new dates in this study; filled circles are *in situ* fossil occurrences, open circles are float specimens; TOC_{wr} denotes Total Organic Carbon measured from whole rock; Sp. = Spelae; Pac. = Pacificum; exp. = exposure.

medium- to thick-bedded Nizina Formation, which together form a ∼1100 m-thick succession deposited during Carnian to late Norian times (Armstrong et al., 1969). During the Norian, thermal subsidence of Wrangellia's northern block is thought to have initiated the drowning of the carbonate platform, resulting in deposition of ∼540 m of calcareous and siliceous mudstones comprising the McCarthy Formation (Greene et al., 2010). The uppermost Triassic and lowermost Jurassic strata of the lower McCarthy Formation are the focus of this study.

4. Materials and methods

We studied the upper Norian to middle Hettangian lower McCarthy Formation along an unnamed tributary of Grotto Creek, located near its headwaters (base of the section: 61°30′13.23″N, 142°26′31.51″W; Fig. 1C), ∼25 km east-northeast of McCarthy, Alaska (Fig. 1C). This section (Grotto Creek section) was originally described by Witmer (2007), who presented a preliminary stratigraphic log and carbon isotope stratigraphy (∼20 m sample spacing) along with sparse paleontological samples and preliminary U–Pb zircon dates of ∼214 and 209 Ma from two bentonites within and stratigraphically below our measured section. To constrain the age of our measured section, we report final high-precision CA-ID TIMS U–Pb zircon dates herein from the bentonite samples studied by Witmer (2007; see SI Table 1.2).

We measured and described 96 m of conformable stratigraphy consisting mostly of buff-weathering, black, carbonaceous, siliceous mudstones and calcareous cherts with textures that alternate between fine mudstones, sandy mudstones, and muddy sandstones. Bentonites occur frequently throughout the middle portion of the section. We placed the 0 m datum of the section (i.e., Fig. 3) at the base of an easily recognizable 5 cm-thick bentonite just below the biostratigraphically defined Norian-Rhaetian boundary. The lower ∼26 m are more resistant and cliff-forming due to the presence of medium-thick beds of sandy mudstone with fine mudstone partings. These alternate with more recessive intervals of fine mudstones. Several beds within this lower interval are laminated. At ∼3 m there is a ∼12 m-high asymmetric fold within an otherwise normally bedded stratigraphic succession (Fig. 4A). We interpret this structure as synsedimentary soft-sediment deformation related to the depositional slope. The upper ∼70 m of the section is a slope-forming succession where thin-bedded fine mudstones are more prevalent than in the lower ∼26 m of the section. The more prominent strata are thin to medium-thick beds of calcareous and siliceous sandy mudstones and fine calcareous cherts. In this upper interval, sedimentary structures have mostly been destroyed by bioturbation.

We collected 70 samples of carbonaceous, siliceous mudstones for $\delta^{13}C_{org}$ and whole-rock total organic carbon (TOC_{wr}) analyses using continuous-flow isotope ratio mass spectrometry (SI Text 1), and four bentonite samples for zircon U–Pb CA-ID TIMS analysis (SI Text 1–3). Additionally, we collected 30 samples for conodont analysis and 103 *in situ* and float macrofossil specimens (ammonoids, bivalves, and hydrozoans) from 51 fossiliferous horizons. Fossils are

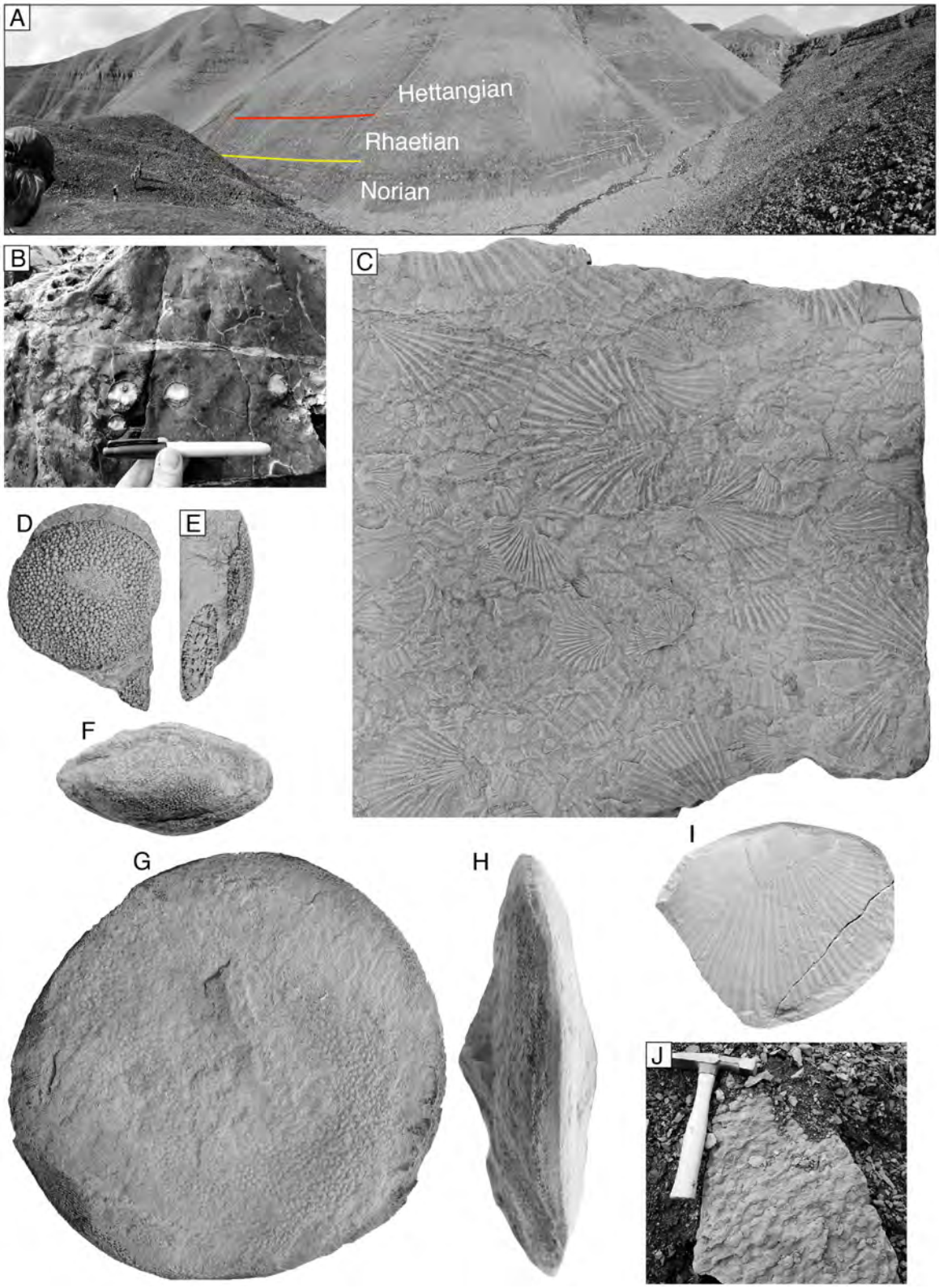

Fig. 4. Photographs of selected strata and specimens in the lower McCarthy Formation, Grotto Creek section. Fossil horizons refer to stratigraphic location in Fig. 3. **A.** Field photograph of the Norian-Rhaetian Boundary (NRB; yellow line) and Triassic-Jurassic Boundary (TJB; red line) intervals; asymmetric fold at right is ∼12 m high. **B.** Field photograph of the middle to late Norian spherical hydrozoan *Heterastridium conglobatum* at −17.67 m in the section; *in situ* between fossil horizons 11 and 12 on Fig. 3 (specimen not collected). **C.** *Monotis subcircularis* (multiple) *in situ* at fossil horizon 6, Cordilleranus Zone, late Norian, natural size. **D and E.** *Heterastridium disciforme* float at fossil horizon 2, middle to late Norian, natural size (D, surface view; E, longitudinal view). **F.** Longitudinal view of *Heterastridium disciforme*, float at fossil horizon 2, middle to late Norian, natural size. **G and H.** *Heterastridium disciforme* float at fossil horizon 2, middle to late Norian, natural size (G, surface view; H, longitudinal view). **I.** *Monotis* cf. *alaskana*, float at fossil horizon 4, Cordilleranus Zone, late Norian, natural size. **J.** Field photograph showing many discoid specimens of *Heterastridium disciforme in situ* at −15.23 m (fossil horizon 12, Fig. 3), middle to late Norian.

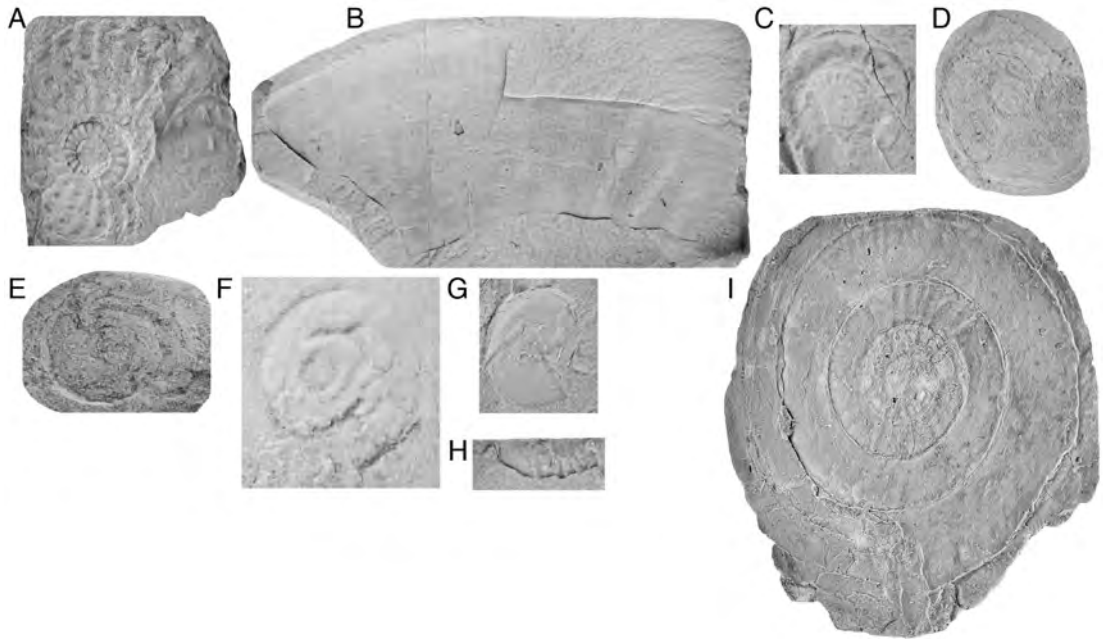

Fig. 5. Selected ammonoids from the McCarthy Formation at Grotto Creek, Alaska. Fossil horizons refer to stratigraphic position in Fig. 3; all specimens natural size unless indicated (e.g., ×2). **A.** *Sagenites* sp. 1, fossil horizon 18, Cordilleranus Zone, late Norian. **B.** *Transipsiloceras* sp., fossil horizon 47, Polymorphum Zone, lower Hettangian. **C.** *Pleuroacanthites* cf. *biformis*, fossil horizon 50, Mulleri to Pleuroacanthitoides zones, middle Hettangian (×2). **D,** *Rhacophyllites debilis*, fossil horizon fossil horizon 14, Columbianus to Crickmayi, late Norian-Rhaetian (×2). **E.** ?*Psiloceras* sp., fossil horizon 40, Spelae to Pacificum zones, lower Hettangian. **F.** *Psiloceras* cf. *tilmanni*, fossil horizon 41, Spelae to Pacificum zones, lower Hettangian (×2). **G.** *Placites polydactylus*, fossil horizon fossil horizon 31, Amoenum Zone, Rhaetian. **H.** *Vandaites* cf. *suttonensis*, fossil horizon 27, Amoenum to Crickmayi zones, Rhaetian (moldic impression). **I.** *Psiloceras polymorphum*, fossil horizon 45, Polymorphum Zone, lower Hettangian.

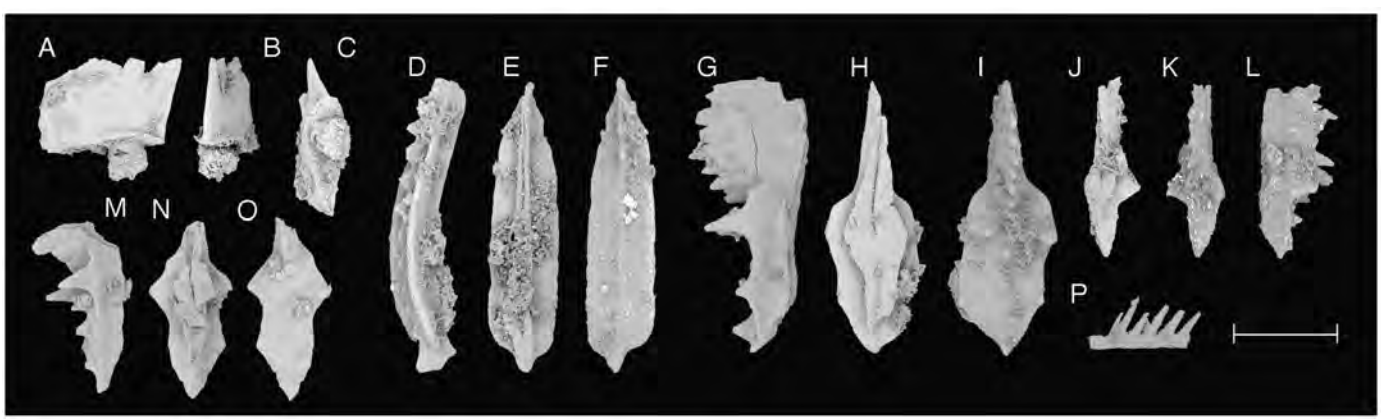

Fig. 6. Conodonts from the McCarthy Formation at Grotto Creek, Alaska. Fossil horizons refer to stratigraphic location in Fig. 3; Scale bar = 200 μm. **A-C,** *Misikella hernsteini*, fossil horizon 11, GSC Type No. 139577, from GSC cur. no. V-016700, late Norian. **D-F.** *Norigondolella steinbergensis*, fossil horizon 11, GSC Type No. 139578, from GSC cur. no. V-016700, late Norian. **G-I.** *Mockina englandi*, fossil horizon 32, GSC Type No. 139579, from GSC cur. no. V-016722, Rhaetian. **J-L.** *Mockina bidentata*, fossil horizon 34, GSC Type No. 139580, from GSC cur. no. V-016725, Rhaetian. **M-O.** *Mockina mosheri* morphotype B *sensu* Carter and Orchard, fossil horizon 32, GSC Type No. 139581, from GSC cur. no. V-016722, Rhaetian. **P.** *Neohindeodella* sp., fossil horizon 39, GSC Type No. 139582, from GSC cur. no. V-016726, Hettangian.

preserved as whole-body specimens and as internal and external molds.

Ammonoid zonation follows Tozer (1994) for the Upper Triassic and Taylor et al. (2001) for the Lower Jurassic, applicable to assemblage zones. Paleontological data are presented in Figs. 3–6, geochemical data in Figs. 3, 7, and 8, and supplementary files contain expanded methodologies, expanded results, and interpretation of geochronology analytical details (SI Text 1–4; SI Fig. 1; SI Tables 1–5). Collected paleontological specimens are curated at the Wrangell-St. Elias National Park and Preserve, with corresponding collections permit numbers (see acknowledgments and SI Table 1.1).

Magnetostratigraphy was not attempted on the Grotto Creek Section. Previous studies by Coe et al. (1985) and Hillhouse and Coe (1994) have shown generally that while Mesozoic volcanic rocks of northern Wrangellia most likely preserved their primary signal, the interbedded and overlying sediments (viz., Cretaceous and Tertiary) have most likely been re-magnetized. Stamatakos et al. (2001) also reinforced these findings by showing that while Cretaceous strata exposed ∼20 km south of Grotto Creek at MacColl Ridge are not remagnetized, the sediments in the Grotto Creek section (i.e., those lying within the outcrop belt of Neogene volcanics/intrusions known as the Wrangell arc) have likely had their paleomagnetic record reset. This is further bolstered by preliminary Rock-Eval pyrolysis data from the McCarthy Formation by Witmer (2007, p. 29, Appendix C) showing high maturity and T_{max} values from 461 to 482 °C. Altogether, this evidence suggests that the McCarthy Formation may not be a suitable candidate for magnetostratigraphic analysis.

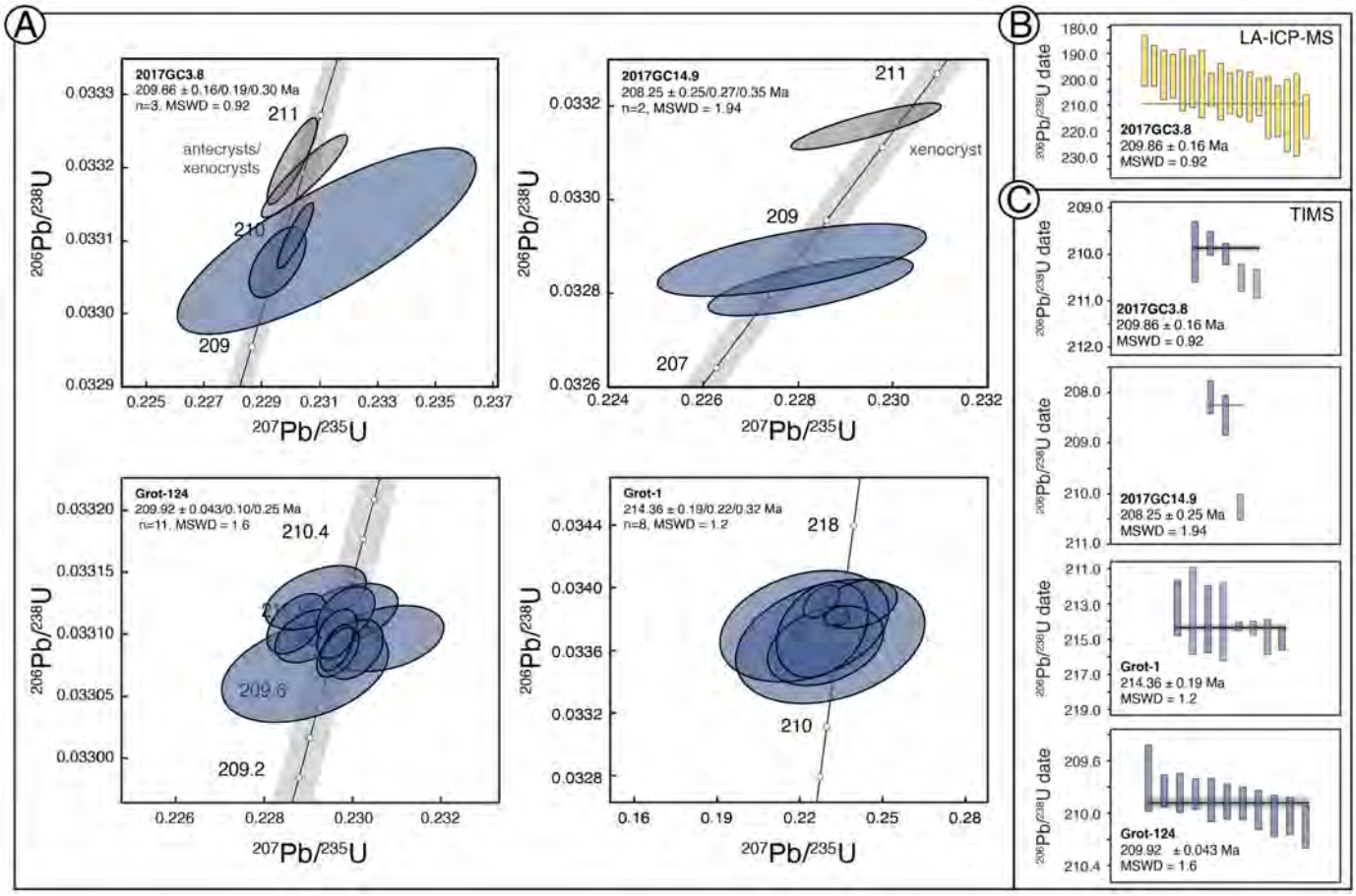

Fig. 7. A. Th-corrected single grain CA-ID-TIMS zircon data for sampled ash beds in the Grotto Creek section. Results shown as blue error ellipses are 2σ and provide the basis for age estimates. Data for older grains inferred to be antecrysts and/or xenocrysts are plotted as grey error ellipses. Two inherited grains (z21, z23) and a single low-precision analysis (z27) were excluded from sample Grot-1; as well as a relatively imprecise result (z18) from 2017GC3.8. Ages along concordia are in Ma, and gray bands (on concordia) show 2σ uncertainties based on decay-constant uncertainties of $^{238}U = 0.107\%$ and $^{235}U = 0.136\%$ (Jaffey et al., 1971). Reported dates are weighted mean $^{206}Pb/^{238}U$ dates—uncertainties are reported as internal/internal + tracer calibration/internal + tracer calibration + decay constant uncertainties. Concordia uncertainties are too small to see for Grot-1. **B and C.** Age distribution data for all bentonite samples in the Grotto Creek section **(B)** is LA-ICPMS U–Pb data from 2017GC3.8 and **(C)** is CA-ID-TIMS U–Pb data from all four bentonite samples. **B and C** show $^{206}Pb/^{238}U$ distributions that are in-line with crystals from a primary ash bed, rather than a volcaniclastic sandstone containing population(s) of significantly older zircon grains.

5. Results

Paleontological data from the base of the section, below reported carbon isotope values, show that the bivalve *Monotis* (*M.* cf. *alaskana*, *M. subcircularis*, and *M.* sp.) occurs in abundance from −30 m to ∼−19 m, with the highest occurrence as float at −18.85 m (Fig. 3). At −18.65 m, the conodonts *Mockina* sp., *Norigondolella steinbergensis*, and *Misikella hernsteini* were recovered along with float ammonoids *Rhacophylites debilis* (−20.6 to ∼−4 m). At −15.23 m, there is a narrow ∼0.5 m-thick interval with abundant *in situ* species of the hydrozoan *Heterastridium*, the spheroidal form *H. conglobatum* (Fig. 4B), and the flattened discoidal form *H. disciforme* (Fig. 4D–H, J). Species identification of this group is based on revised systematic descriptions in Senowbari-Daryan and Link (2019). The conodont *Mockina* sp. was recovered at −10.1 m and float specimens of the bivalve ?*Leptochondria* sp. and the ammonoid *Rhacophylites debilis* at −4 m.

From −2.1 to 6.95 m, the conodont *Mockina bidentata* was recovered close to a float ammonoid *Sagenites* sp. 1 (∼−2.1 m; Fig. 3), with *in situ* and float specimens of the bivalve *Agerchlamys boellingi* overlapping with ammonoids *Rhacophylites debilis* and *Sagenites* sp. 2 (2.95 to 4.1 m). At 4.15 m the ammonoid *Vandaites* cf. *suttonensis* was found *in situ* along with the ammonoids ?*Paracochloceras* cf. *amoenum* and *Placites polydactylus* and *Agerchlamys* cf. *boellingi* (4.95 to 6.95 m). This is followed by a ∼20 m-thick interval with several *in situ* and float taxa including: *Agerchlamys boellingi*, *Mockina bidentata*, *Mockina englandi*, *Mockina mosheri* morphotype B, *Norigondolella* sp., *Sagenites* cf. *minaensis*, and *Choristoceras rhaeticum*.

At 29.42 m, the ammonoid ?*Psiloceras* sp. was recovered *in situ* along with the conodont *Neohindeodella* sp. followed by float and *in situ* occurrences of the ammonoid *Psiloceras tilmanni* (∼33.95 to 35.45 m), *Agerchlamys* cf. *boellingi* (∼37.95 to 38.95 m), and float specimens of the ammonoid *Psiloceras polymorphum* (∼40.95 to 45.95 m). Near the top of the section, the ammonoids *Transipsiloceras* sp., *Nevadaphyllites* aff. *compressus*, and *Pleuroacanthites* cf. *biformis* were recovered along with *Agerchlamys* cf. *boellingi* (spanning ∼45.95 to 64.75 m; Fig. 3).

The four sampled bentonites were collected from (i) 50 m above the base of the McCarthy Formation (i.e., Grot-1, Fig. 7, occurring below the base of our measured section); (ii) approximately −6 to 0 m in our section (i.e., Grot-124, position approximated based on correlation with Witmer, 2007, discussed below in section 6.1); (iii) 0 m (i.e., 2017GC3.8); (iv) 11.07 m (i.e., 2017GC14.9) (Figs. 3, 7). Bentonites (i) and (ii) are finalized data originally collected by Witmer (2007) and (iii) and (iv) are new to this study. We interpret the bentonites as four separate volcanic events and associated settling of volcanic ash through the water column with no sedimentary evidence for reworking or abrasion of the grains. The bentonites form yellow-weathering thin (<10 cm)

recessive beds and contain elongate euhedral to subhedral crystals with minor inclusions. Well-developed zoning patterns are present in imaged grains (sample 2017GC3.8, SI Fig. 1), and tight clusters of dates occur from analyzed grains within each respective sample (see SI text 2, 3 for an expanded justification for our interpretation of the bentonites).

U–Pb chemical abrasion-isotope dilution (CA-ID) TIMS analysis were carried out at the University of British Columbia (UBC) and the Massachusetts Institute of Technology (MIT). All samples were run using the EARTHTIME 535 tracer (calibration v. 3), thus minimizing interlaboratory biases. Complete results, photomicrographs and/or cathodoluminescence images of zircon grains, and laser ablation-derived trace element concentration data are presented as Supplemental Information (SI Text 2; Fig. 1; Tables 2–5).

Eleven single-grain analyses from sample Grot-124 yielded overlapping Th-corrected $^{206}Pb/^{238}U$ dates from 210.10 ± 0.16 to 209.73 ± 0.25 Ma (Fig. 7A), with a weighted mean of 209.92 ± 0.043 Ma (MSWD = 1.6), which we interpret as the eruption age of the sample (reported uncertainties are 2-sigma internal). Ten single-grain analyses from sample Grot-1 yielded a range of Th-corrected $^{206}Pb/^{238}U$ dates from 245.8 ± 2.0 to 213.2 ± 1.6 Ma (excluding a single low precision analysis, z27). Eight of the 10 analyses shown on Fig. 7A overlap within uncertainty with a Th-corrected weighted mean $^{206}Pb/^{238}U$ date of 214.36 ± 0.19 Ma (MSWD = 1.2), which we interpret as the eruption age of this sample—the two older zircon grains (246–221 Ma) are likely inherited (not shown on Fig. 7). Six dated grains from sample 2017GC3.8 (0 m, Fig. 3) yielded dates of 210.60 ± 0.31 to 209.73 ± 0.25 Ma. The data comprises distinct younger (3 results) and older (2 results) groupings, and a relatively imprecise result (not plotted, Fig. 7A) that spans the two clusters. A weighted mean $^{206}Pb/^{238}U$ date of 209.86 ± 0.16 Ma for the younger cluster is interpreted as the best estimate age, with older grains interpreted as antecrysts or xenocrysts. For sample 2017GC14.9 (11.07 m, Fig. 3), two younger grains yield a weighted mean $^{206}Pb/^{238}U$ date of 208.25 ± 0.25 Ma, and a single older grain is likely a xenocryst (Fig. 7).

TOC_{wr} values range ∼0.5–3 wt%, with an average of 1.5 wt% (Fig. 3). TOC_{wr} is variable through the upper Norian (up to ∼4.15 m) in the section, followed by a trend towards lower values in the Rhaetian (∼19.95 m) before gradually increasing across the TJB, peaking at 2.7 wt% (∼31.95 m; Fig. 3). Values stabilize through the Spelae-Pacificum zones and remain below 2 wt% (apart from one value of 2.6 wt% at 51.97 m) to the top of the section. $\delta^{13}C_{org}$ values become gradually less negative from −29‰ to −28‰ through the Rhaetian with two decreases occurring in close proximity to the TJB: the first from −27.56‰ to −29.22‰ (26.42 to 30.03 m), and a second from −27.92‰ to −29.26‰ (32.46 to 35.97 m). Above this, $\delta^{13}C_{org}$ values gradually increase from ∼−∼29‰ to −27.5‰ at the top of the measured section (Fig. 3).

6. Discussion

Our data from the Wrangellia terrane represent an important addition to the global database of Upper Triassic to Lower Jurassic successions. Biostratigraphy shows a complete (i.e., Cordilleranus to Mulleri) ammonite zonation in the Grotto Creek section with no obvious long breaks in sedimentation, suggesting a complete record from upper Norian to lower-middle Hettangian. These data not only improve the resolution of timescale calibrations, but also provide a more holistic understanding of biogeochemical dynamics associated with the ETE from Panthalassa. Here, we establish the Grotto Creek section as an important succession with respect to the (i) debated long vs. short duration of the Rhaetian, (ii) paleontological and geochemical trends across the TJB, and (iii) implications of the VGS and controlling mechanisms of the ETE.

6.1. A case for a long Rhaetian

Precise quantification of the duration of the Rhaetian Stage is pivotal for understanding the timing of the events surrounding the ETE. At present, various lines of indirect evidence are used to argue for the initiation of CAMP magmatism prior to the oldest dated igneous bodies (e.g., Davies et al., 2017). These include seismites, basalt-derived sediments directly below CAMP basalts, and eustatic sea-level fall during the Rhaetian, as evidence of short-term climatic cooling (induced by volcanic SO_2) and the VGS (e.g., Schoene et al., 2010). Importantly, this early initiation is invoked to explain possible diachroneity between mass extinction in the marine and terrestrial records (e.g., Pálfy et al., 2000), and therefore it is essential to better constrain the duration of the Rhaetian.

In the Grotto Creek section the NRB (Fig. 4A, yellow line) occurs at 4.15 m, just above the ∼12 m-high soft-sediment deformation fold (Fig. 4A at right), temporally constrained through biostratigraphic data and the ∼209 Ma U–Pb zircon CA-ID-TIMS dates from bentonites in the lower McCarthy Formation (Figs. 3, 7; SI Text 2, SI Fig. 1, SI Tables 1–5).

From the section base to 4.15 m, a late Norian Cordilleranus Zone age is indicated by occurrences of *Monotis*, *Heterastridium*, ammonoids, and age-specific conodonts (Figs. 2–6). The last *in situ Monotis* occurs at −24.87 m, uppermost float *M. subcircularis* at −18.85 m, and lowest *in situ Heterastridium* at −15.23 m. According to Senowbari-Daryan and Link (2019), previous accounts of *Heterastridium* from the Carnian and Rhaetian stages are doubtful, and this genus is restricted to the Norian Stage. From 3.24 to 4.15 m, *in situ Rhacophyllites debilis* overlaps with the lowest *in situ Agerchlamys boellingi* and the strictly Rhaetian ammonoid *Vandaites* cf. *suttonensis* (at 4.15 m), marking the NRB at Grotto Creek (∼4 m, Fig. 3).

The abundance of bentonite beds (orange lines in Fig. 3) in this part of the section hampers the exact placement of the dated bentonite bed collected by Witmer (2007; i.e., Grot-124, Figs. 3, 7, 209.92 ± 0.043 Ma) within our measured section. Witmer (2007) noted that Grot-124 occurs 19 m above the last occurrence of *Monotis*. This is estimated at ∼−6 to 0 m in our section, bounded by our uppermost measured *in situ Monotis* (at −24.87 m) and the uppermost float *M. subcircularis* (−18.83 m); this is demarcated by a dashed, red-lined box of uncertainty in Fig. 3. Stratigraphically, this interval is just below our new dates of 209.86 ± 0.16 Ma and 208.25 ± 0.25 Ma from 0 and 11.07 m, respectively, which span the NRB (∼4 m, Fig. 3). The characteristics of the zircons (SI Text 2, 3; SI Fig. 1) and the tight clusters of dates (Fig. 7) indicate a primary magmatic age. Overall, this is consistent with a long duration (∼8 Ma) for the Rhaetian from ∼209–201.4 Ma.

The interpretation presented here of a long duration Rhaetian Stage is similar to that derived from the Steinbergkogel section in Austria (e.g., Li et al., 2017; Fig. 1), which uses *M. posthernsteini s.l.* for the NRB datum, but in the Grotto Creek section we use the first occurrence of the ammonoid *Vandaites suttonensis* as the NRB indicator (which has been shown to be restricted to the Rhaetian; Tozer, 1994; e.g., Fig. 2). In the Grotto Creek section, samples collected for conodont analysis from this interval were barren and no specimens of *Misikella posthernsteini* (*s.s.* or *s.l.*) were recovered. A dominance of late Norian taxa low in the section followed directly by *in situ Agerchlamys boellingi* and *Vandaites* cf. *suttonensis* at ∼3.9 m, with a variety of Rhaetian-restricted taxa above, however, strongly support the placement of NRB.

Our duration for the Rhaetian appears at odds with the record from Levanto in Peru where similar lines of evidence are used in support of a short-duration Rhaetian (i.e., last occurrence of *Monotis* below *Vandaites* with no reported occurrence of NRB-defining conodont *M. posthernsteini s.s.* or *s.l.*; Wotzlaw et al., 2014). An important detail concerning the Levanto succession, however, is that

Wotzlaw et al. (2014; Fig. 2) report primary magmatic dates of ∼205 Ma from bentonites that occur ∼5 m above the last occurrence of *M. subcircularis* and ∼50 m below the first occurrence of *Vandaites*. At Grotto Creek, primary magmatic dates of ca. 209 to 208 Ma were derived from bentonites that occur above the last occurrence of *M. subcircularis* and bracket the first occurrence of *Vandaites* cf. *suttonensis* (i.e., Figs. 3, 7B). Per Wotzlaw et al. (2014) and using a similar argument as Galbrun et al. (2020), if the extinction of *Monotis* was relatively globally synchronous, then the discrepancy between the Grotto Creek and Levanto stratigraphies and our probable primary magmatic dates suggest that the Levanto section contains unidentified hiatus(es) and/or is condensed over the Norian-Rhaetian transition.

In summary, it becomes apparent that given the wide array of complicating factors surrounding the NRB (i.e., current definition and potential stratigraphic complexities with the existing records), the definition should be revised to include multiple lines of data that can be applied globally. As previously noted, various correlations of marine strata to the Newark-APTS have been used to argue for both a long and short Rhaetian. The new U–Pb dates from Grotto Creek place the NRB in the reverse or normal polarity intervals of the E17 chron of Newark-APTS 2017 (Kent et al., 2017). This correlation supports age models that lack a gap in the Newark succession (e.g., Kent et al., 2017) and also that the first appearance of *Misikella posthernsteini s.l.* and not *Misikella posthernsteini s.s.* marks the NRB (e.g., Krystyn et al., 2007).

Carbon isotope stratigraphy has recently been suggested to provide an additional constraint, as recent work has suggested that a NCIE may occur in the NRB interval (Rigo et al., 2020). Although rigorous evaluation of the geographic extent of this CIE is outstanding, the negative values at −2.79 and 0.22 m in the Grotto Creek section may correlate with this NRB NCIE. Since our data do not extend below this interval, we cannot at present confidently identify this trend at Grotto Creek as being correlative with this suspected NRB NCIE. Nevertheless, a new multi-faceted definition of the NRB is needed to provide a means to overcome shortcomings in any one kind of datum and provide a more utilitarian means to correlate strata globally.

6.2. The Triassic-Jurassic boundary interval at Grotto Creek

A TJB transition interval is defined with our combined paleontological and geochemical ($\delta^{13}C_{org}$) data from the Grotto Creek section. Overlying the NRB, there is a ∼22 m-thick interval (up to 26.65 m) that contains Rhaetian ammonoids and an assortment of Norian-Rhaetian conodonts and bivalves (Figs. 3, 5, 6). While *Choristoceras rhaeticum* is known to be restricted to the Crickmayi Zone (Tozer, 1994), its occurrence at 26.65 m is from float and therefore we cannot currently designate a Crickmayi Zone boundary. Furthermore, the lowest *in situ Agerchlamys boellingi* is 0.08 m below the NRB, which places this species within the uppermost Norian, in agreement with previous accounts for a Late Triassic origin (e.g., Larina et al., 2019) and refuting its utility as a defining species of the TJB.

From 29.42 to 35.46 m, the TJB is defined based on the co-occurrence of the lowest *in situ* strictly Jurassic genus *Psiloceras* (i.e., ?*Psiloceras*) and the highest *in situ* conodont (*Neohindeodella* sp.), both at 29.42 m, and the lowest *in situ Psiloceras* cf. *tilmanni* at 35.46 m (Fig. 3 shaded region; Fig. 4A red line). The poor preservation of ?*Psiloceras* (at 29.42 m) above the highest float *Choristoceras rhaeticum* precludes unequivocal delineation of the TJB, which requires a TJB interval of ∼6 m in the section. Regardless, the occurrence of *P*. cf. *tilmanni* is a robust indication of the lower Hettangian (Figs. 2A, 5), which marks the upper limit (of the ∼6 m TJB interval). This is followed by two *in situ* occurrences of *A*. cf. *boellingi* and an assortment of float ammonoids from the Pacificum (e.g., *Psiloceras pacificum*), Polymorphum (e.g., *Psiloceras polymorphum* and *Transipsiloceras* sp.), and Mulleri (e.g., *Pleuroacanthites* cf. *biformis*) zones representing the lower to middle Hettangian (Figs. 2, 5).

Organic carbon isotopes in the uppermost Rhaetian record a ∼1.3‰ positive carbon isotope excursion (PCIE) from 23.69 to 26.42 m (Fig. 3). This is followed by an abrupt NCIE of 1.7‰ that is broad in character (i.e., ∼15 m in stratigraphic thickness), which begins at 26.42 m and extends through to the top of the Spelae–Pacificum zones at 40.94 m (Figs. 3, 8). Within this broad NCIE, two further NCIEs occur with a magnitude of 1.7‰ and ∼1.3‰ at 26.42 and 32.46 m, respectively. Altogether, this broad trend in organic carbon isotope values is consistent with other global TJB records (Fig. 8, see discussion below).

6.3. Global vs. regional carbon cycle perturbations and the ETE

Available records of the TJB interval show numerous small-magnitude fluctuations in organic carbon isotopes. The stratigraphic and geographic distributions of these CIEs have implications regarding their underlying drivers and utility for regional to global correlation. Here, we briefly review some of the existing carbon isotope records in attempt to reconcile important differences and help develop a more complete understanding of environmental changes enveloping the ETE.

Most studies of the ETE and TJB $\delta^{13}C_{org}$ records are from the westernmost Tethys and have signatures that commonly delineate two NCIEs: the first occurs below the TJB, commonly referred to as the *initial* NCIE (∼2–5‰), and the second, referred to as the *main* isotope excursion (∼5‰), occurs just above the base of the Jurassic (Hesselbo et al., 2002). Additionally, the available terrestrial carbon-isotope records across this interval (i.e., East Greenland, Poland, and Denmark) show a similar *initial* NCIE below the TJB with a *main* NCIE above (e.g., Steinthorsdottir et al., 2011; Pieńkowski et al., 2020; Korte et al., 2019).

Recent work by Ruhl and Kürschner (2011), Lindström et al. (2017), and others expand the number of NCIEs to three based on ammonoid and palynoflora occurrences in sections primarily from the westernmost Tethys, identifying them (in stratigraphic order) as the: Precursor (or Marshi; correlative within the last occurrence of the Rhaetian ammonite *Choristoceras marshi*), Spelae (correlative with the *initial* NCIE occurring within the earliest Hettangian), and top-Tilmanni (correlative with the *main* NCIE occurring at a slightly higher position in the early Hettangian). Most recently, Kovács et al. (2020) show many small-scale anomalies in both the $\delta^{13}C_{carb}$ and $\delta^{13}C_{org}$ records across this TJB transition from the western Tethys shelf (Csővár, Hungary).

To date, however, the three larger-magnitude and multiple higher-frequency, smaller-magnitude NCIEs observed in the Tethyan records have not been clearly identified within Panthalassan successions. Here, we assess features of the TJB organic carbon isotope record that can be delineated and reliably correlated across Panthalassa and then assess potential correlations to records from the Tethys (Fig. 8). This opens the door to a discussion concerning the ubiquity of these smaller NCIEs and helps to delineate regional *versus* global signals across the TJB organic carbon isotope record.

Compilation TJB data from Wrangellia and Eastern Panthalassa show a PCIE of ∼1.5‰ to ∼2.0‰ that occurs in the upper Rhaetian (green shading on Fig. 8), which appears of larger (∼5‰) magnitude in Central Panthalassa (e.g., deep-water chert deposits in Japan). This is followed by a NCIE that initiates toward the end of the Rhaetian near the top of the Crickmayi/Marshi ammonite zone beginning just at, or before, the extinction interval that precedes the TJB (blue shading on Fig. 8). The overall magnitude of the NCIE varies from 1.66‰ to 4.94‰ and appears to contain higher-order oscillations in most of the Panthalassan successions.

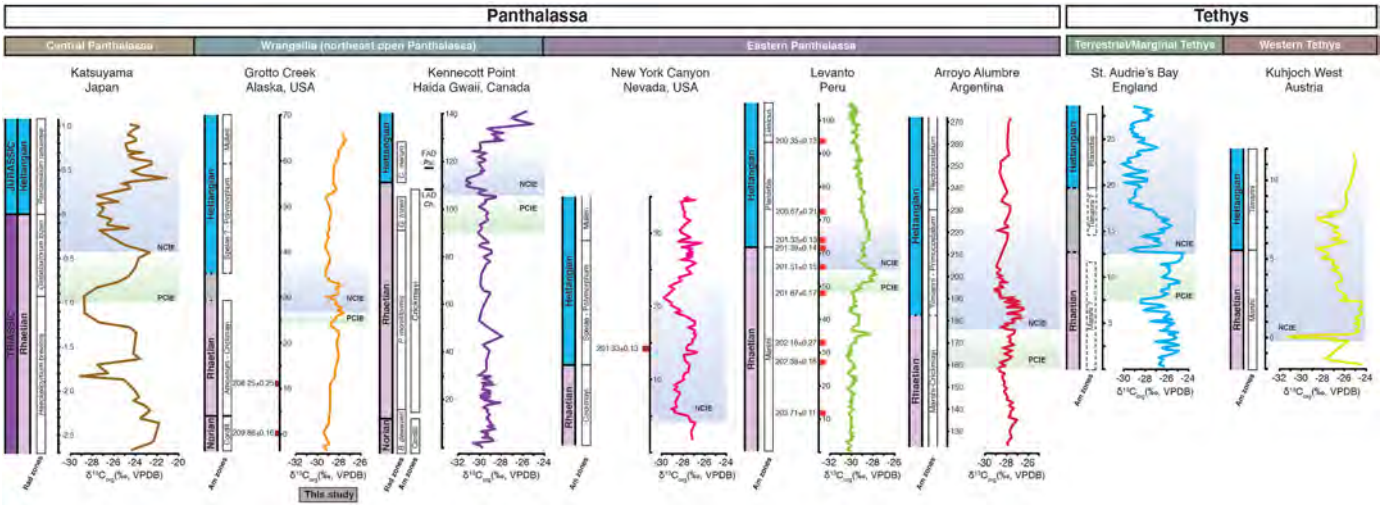

Fig. 8. Composite carbon isotope data across the TJB interval from Panthalassa and northwestern Tethys oceans showing the broadly defined PCIE and NCIE intervals. Colored $\delta^{13}C_{org}$ data curve refers to locality in Fig. 1A. Red hash marks denote position of sampled bentonites that provide new and previously established U–Pb age constraints. See Korte et al. (2019), Ruhl et al. (2020), and Du et al. (2020) for individual section citations. Rad = radiolarian, Am = Ammonoid, Cordill. = Cordilleranus, Sp. = Spelae, Pac. = Pacificum, *Ch.* = *Choristoceras*, *Psi.* = *Psiloceras*, FAD = First Appearance Datum, LAD = Last Appearance Datum, Pol. = *Polymorphum*, and VPDB = Vienna PeeDee Belemnite.

In Nevada, however, it should be noted that existing data do not extend low enough in the stratigraphy to confirm a PCIE. Timing of the initiation of the PCIE and NCIE are constrained by the Peruvian Levanto section, where two bentonite beds at these intervals have been dated to 201.87 ± 0.17 Ma and 201.51 ± 0.15 Ma, respectively.

We compare these features of Panthalassa to those recorded in the Tethys and suggest a more simplified global correlation. Here, we use the St. Audrie's Bay (England) and Kuhjoch West (Austria) records as points of reference, as nearly all other Tethyan records are compared to these (e.g., Korte et al., 2019; Kovács et al., 2020). We note, however, that these records are inherently problematic: the TJB transition at St. Audrie's Bay records a transition from continental/marginal marine to fully marine environments, and a shear zone deforms the Kuhjoch West section at the stratigraphic interval that records the onset of the *main* NCIE (Ruhl et al., 2009; Palotai et al., 2017).

Nevertheless, in comparison to these schemes, the PCIE from Panthalassa corresponds to a ∼5.5‰ PCIE in the upper Rhaetian at St. Audrie's Bay that is just below the *initial* (= Spelae CIE) and well below the *main* (= top-Tilmanni CIE). A similar feature occurs broadly at the same level in many other Tethyan $\delta^{13}C_{org}$ records (e.g., Lindström et al., 2017; Korte et al., 2019). Specifically, at Kuhjoch West, an *initial* NCIE occurs below 0 m and the *main* NCIE at ∼2.5 m in section (Fig. 8; Ruhl et al., 2009; Hillebrandt et al., 2013).

The overlying NCIE spans the uppermost Rhaetian into the Hettangian, corresponding to (and containing) the *initial* (Spelae) and *main* (top-Tilmanni) CIEs. These events are likely higher-frequency oscillations contained within a temporally broader NCIE. To this point, the St. Audrie's Bay and Kuhjoch West records also contain other higher-frequency $\delta^{13}C$ oscillations (or NCIEs) of similar magnitude (up to 3‰) stratigraphically above and below the previously described *initial* and *main* NCIEs.

Given that these higher-order features observed in the Tethys either do not appear or are subdued in the open ocean records of Panthalassa, there exists at present a need for a more conservative definition of the global $\delta^{13}C_{org}$ record of the TJB interval. This new definition should be centered on open ocean records and account for local dynamics that either magnify $\delta^{13}C_{org}$ in regional records of individual sedimentary basins or dampen global signals.

Deciphering such global *versus* regional signals across the TJB has important implications for environmental changes and carbon cycle dynamics controlling the ETE. The driving mechanisms at the onset of the broader NCIE are coincident (within error) with the first major evidence of CAMP volcanism dated to 201.566 ± 0.031 Ma (Blackburn et al., 2013). Alternatively, Davies et al. (2017) emphasized the role of subvolcanic intrusions whose emplacement preceded the first eruptive phase and may have contributed degassing of greenhouse gases through contact with organic-rich sedimentary rocks. Regardless, input of ^{12}C-enriched carbon to the ocean-atmosphere from CAMP has long been invoked as the driver of these NCIEs.

The finer-scale NCIEs, if global, could reflect inputs of ^{12}C-enriched carbon to the ocean and atmosphere from discrete eruptive phases of CAMP or other carbon cycle feedbacks (e.g., methane releases, global declines in productivity, response of terrestrial carbon cycling; e.g., Heimdal et al., 2020). This is substantiated by a second known eruptive phase at 201.274 ± 0.032 Ma (Blackburn et al., 2013), which potentially correlates in time to the initiation of a second negative shift in $\delta^{13}C_{org}$ at Levanto (e.g., ∼65 m in that section; Fig. 8). Alternatively, if higher-order NCIEs are only regionally correlative (i.e., do not occur in open-ocean Panthalassan environments), this could indicate a dominance of local/regional influences on the $\delta^{13}C_{org}$ record, which should not be factored into interpretations and modeling of the global carbon cycle.

Therefore, it becomes evident that determining the global *versus* regional nature of isotope excursions surrounding the TJB remains an outstanding and important challenge, critical to understand the end-Triassic mass extinction. We posit that new multi-proxy, multi-lithology, and higher-resolution studies are required to fully address the underlying mechanisms, magnitudes, and outstanding uncertainties of the carbon isotope record around the ETE.

7. Conclusions

Paleontological and geochemical data were collected from the Grotto Creek section (Wrangell Mountains, Alaska) representing undisturbed deposition on the oceanic plateau of Wrangellia in open Panthalassa during Late Triassic to Early Jurassic time. Data suggest (i) an upper Norian (Cordilleranus Zone) succession spanning the lower ∼34 m of the section, well constrained by abundant occurrences of *Monotis*, *Heterastridium*, and age-specific conodonts; (ii) the NRB at 4.15 m marked by the appearance of the Rhaetian heteromorph ammonoid *Vandaites* cf. *suttonensis*, supported by overlying Rhaetian-restricted ammonoids and assorted

Norian–Rhaetian conodonts and bivalves; (iii) three new primary magmatic U–Pb CA-ID TIMS dates of 209.92 ± 0.043, 209.86 ± 0.16 and 208.25 ± 0.25 Ma from bentonites that straddle the NRB, suggesting a boundary age of ∼209 Ma (in line with a longer, ∼8 Ma, Rhaetian); (iv) a stratigraphically continuous TJB transition interval from 29.42 to 35.46 m marked by ?*Psiloceras* sp., *Neohindeodella* sp., and *P*. cf. *tilmanni*, and followed by an assortment of float ammonoids from the early to middle Hettangian Polymorphum to Mulleri zones; and (v) a new, simplified, interpretation of the $\delta^{13}C_{org}$ record across the TJB, whereby a PCIE of variable magnitude is directly followed by an NCIE that is subdued in open-ocean Panthalassa but contains many second-order features in the Tethys and marginal Panthalassa, potentially highlighting regional carbon cycle dynamics during a time of global carbon cycle perturbation. This combined biostratigraphic and geochemical record of the Upper Triassic to Lower Jurassic succession at Grotto Creek (Alaska) is the best-known record of the NRB and TJB intervals from not only Wrangellia, but from all the other terranes in western North America.

CRediT authorship contribution statement

Andrew Caruthers: Conceptualization, Funding acquisition, Investigation, Formal analysis (paleontological), Writing – original draft, Writing – review & editing. **Selva Marroquín**: Investigation, Formal analysis (geochemical), Methodology, Writing – original draft, Writing – review & editing. **Darren Gröcke**: Formal analysis (geochemical), Methodology, Writing – review & editing. **Martyn Golding**: Formal analysis (paleontological), Methodology, Writing – review & editing. **Martin Aberhan**: Formal analysis (paleontological), Methodology, Writing – review & editing. **Theodore Them II**: Investigation, Writing – original draft, Writing – review & editing. **João Trabucho-Alexandre**: Investigation, Writing – original draft, Writing – review & editing. **Yorick Veenma**: Investigation, Writing – review & editing. **Jeremy Owens**: Investigation, Writing – original draft, Writing – review & editing. **Chris McRoberts**: Formal analysis (paleontological), Methodology, Writing – review & editing. **Richard Friedman**: Formal analysis (geochemical), Methodology, Writing – review & editing. **Jeff Trop**: Investigation (original work), Writing – review & editing. **Dominika Szűcs**: Investigation (original paleontological), Writing – review & editing. **József Pálfy**: Investigation (original paleontological), Writing – review & editing. **Benjamin Gill**: Conceptualization, Funding acquisition, Investigation; Formal analysis (geochemical), Writing – original draft, Writing – review & editing.

Declaration of competing interest

The authors declare that they have no known competing financial interests or personal relationships that could have appeared to influence the work reported in this paper.

Acknowledgements

We thank Mark Miller, Morgan Gantz, Desiree Ramirez, and Danny Rosencrans at the Wrangell - St. Elias National Park and Preserve (collections permit numbers WRST-2017-SCI-0004 and WRST-2018-SC1-0005) for access to Grotto Creek and continued support for this project; Paul Claus at Ultima Thule Charters for air support; and Robert B. Blodgett for logistical support. AHC acknowledges Lauren Jaskot for fossil photography. We thank detailed comments and critiques by two anonymous reviewers which led to an improved manuscript. This work was supported by grants from the National Geographic Society (NGS-9973-16) to AHC and the National Science Foundation (EAR-2026926) to AHC, JDO, and BCG. BCG and SMM would like to thank the Virginia Tech College of Science Dean's Discovery Fund for financial support of the fieldwork; SMM would like to thank the Virginia Tech Department of Geosciences, Geological Society of America, Alaska Geological Society, SEPM Society for Sedimentary Geology, and the Paleontological Society for student grants used to fund this work; TRT would like to thank the College of Charleston Faculty Research & Development Committee for financial support of the fieldwork; JDO acknowledges Florida State University Planning Grant and NASA Exobiology (80NSSC18K1532) for financial support of the fieldwork and support by the National High Magnetic Field Laboratory (Tallahassee, Florida), which is funded by the National Science Foundation Cooperative Agreement No. DMR1644779 and the State of Florida; JPTA and YPV would like to thank the Molengraaff fund and SEPM for financial support of the fieldwork; MA would like to thank the DFG-funded Research Unit TERSANE (FOR 2332: Temperature-related Stressors as a Unifying Principle in Ancient Extinctions) for support and Michael Hautmann for discussion of Triassic bivalve taxonomy; MG would like to thank the Geological Survey of Canada GEM 2 Program for financial support of the fieldwork and conodont analyses; JP acknowledges support from the National Research, Development and Innovation Office (Grant No. NN 128702 and K135309); RF acknowledges H. Lin for mineral separation, T. Ockerman and J. Cho for grain mounting and imaging, and M. Amini for laser set-up; and JMT acknowledges the American Chemical Society for financial support of reconnaissance fieldwork, and C. Slaughter and J. Witmer for field assistance.

Appendix A. Supplementary material

Supplementary material related to this article can be found online at https://doi.org/10.1016/j.epsl.2021.117262.

References

Alroy, J., Aberhan, M., Bottjer, D.J., Foote, M., Fürsich, F.T., Harries, P.J., Hendy, A.J.W., Holland, S.M., Ivany, L.C., Kiessling, W., Kosnik, M.A., Marshall, C.R., McGowan, A.J., Miller, A.I., Olszewski, T.D., Patzkowsky, M.E., Peters, S.E., Villier, L., Wagner, P.J., Bonuso, N., Borkow, P.S., Brenneis, B., Clapham, M.E., Fall, L.M., Ferguson, C.A., Hanson, V.L., Krug, A.Z., Layou, K.M., Leckey, E.H., Nürnberg, S., Powers, C.M., Sessa, J.A., Simpson, C., Tomasovych, A., Visaggi, C.C., 2008. Phanerozoic trends in the global diversity of marine invertebrates. Science 321, 97–100. https://doi.org/10.1126/science.1156963.

Armstrong, A.K., MacKevett Jr., E.M., Silberling, N.J., 1969. The Chitistone and Nizina Limestones of part of the southern Wrangell Mountains, Alaska – a preliminary report stressing carbonate petrography and depositional environments. U.S. Geol. Surv. Prof. Pap. 650-D, D49–D62.

Blackburn, T.J., Olsen, P.E., Bowring, S.A., Mclean, N.M., Kent, D.V., Puffer, J., Mchone, G., Rasbury, E.T., Et-touhami, M., 2013. Zircon U-Pb geochronology links Central Atlantic Magmatic Province. Science 340, 941–946. https://doi.org/10.1126/science.1234204.

Blakey, R., 2014. Triassic period. http://www.geologypage.com/2014/04/triassic-period.html.

Carter, E.S., Hori, R.S., 2005. Global correlation of the radiolarian faunal change across the Triassic-Jurassic boundary. Can. J. Earth Sci. 42 (5), 777–790.

Caruthers, A.H., Stanley Jr., G.D., 2008. Late Triassic silicified shallow-water corals and other marine fossils from Wrangellia and the Alexander terrane, Alaska and Vancouver Island, British Columbia. In: Blodgett, R.B., Stanley Jr., G.D. (Eds.), The Terrane Puzzle: New Perspectives on Paleontology and Stratigraphy from the North American Cordillera. In: Spec. Pap. Geol. Soc. Am., vol. 442, pp. 151–179.

Colpron, M., Nelson, J.L., 2009. A Palaeozoic Northwest Passage: incursion of Caledonian, Baltican and Siberian terranes into eastern Panthalassa, and the early evolution of the North American Cordillera. In: Cawood, P.A., Kröner, A. (Eds.), Earth Accretionary Systems in Space and Time. In: Spec. Publ. Geol. Soc. (Lond.), vol. 318, pp. 273–307.

Davies, J.H.F.L., Marzoli, A., Bertrand, H., Youbi, N., Ernesto, M., Schaltegger, U., 2017. End-Triassic mass extinction started by intrusive CAMP activity. Nat. Commun. 8, 15596. https://doi.org/10.1038/ncomms15596.

Du, Y., Chiari, M., Karádi, V., Nicora, A., Onoue, T., Pálfy, J., Roghi, G., Tomimatsu, Y., Rigo, M., 2020. The asynchronous disappearance of conodonts: new constraints from Triassic – Jurassic boundary sections in the Tethys and Panthalassa. Earth-Sci. Rev., 103176.

Galbrun, B., Boulila, S., Krystyn, L., Richoz, S., Gardin, S., Bartolini, A., Maslo, M., 2020. "Short" or "long' Rhaetian? Astronomical calibration of Austrian key sections. Glob. Planet. Change 192, 103253.

Golding, M.L., Mortensen, J.K., Zonneveld, J.P., Orchard, M.J., 2016. U–Pb isotopic ages of euhedral zircons in the Rhaetian of British Columbia: implications for Cordilleran tectonics during the Late Triassic. Geosphere 12, 1606–1616.

Greene, A.R., Scoates, J.S., Weis, D., Katvala, E.C., Israel, S., Nixon, G.T., 2010. The architecture of oceanic plateaus revealed by the volcanic stratigraphy of the accreted Wrangellia oceanic plateau. Geosphere 6 (1), 47–73.

Guex, J., Bartolini, A., Atudorei, V., Taylor, D., 2004. High-resolution ammonite and carbon isotope stratigraphy across the Triassic–Jurassic boundary at New York Canyon (Nevada). Earth Planet. Sci. Lett. 225, 29–41. https://doi.org/10.1016/j.epsl.2004.06.006.

Guex, J., Schoene, B., Bartolini, A., Spangenberg, J., Schaltegger, U., O'Dogherty, L., Atudorei, V., 2012. Geochronological constraints on post-extinction recovery of the ammonoids and carbon cycle perturbations during the Early Jurassic. Palaeogeogr. Palaeoclimatol. Palaeoecol. 346, 1–11. https://doi.org/10.1016/j.palaeo.2012.04.030.

Heimdal, T.H., Jones, M.T., Svensen, H.H., 2020. Thermogenic carbon release from the Central Atlantic magmatic province caused major end-Triassic carbon cycle perturbations. Proc. Natl. Acad. Sci. 117, 11968–11974. https://doi.org/10.1073/pnas.2000095117.

Hesselbo, S.P., Robinson, S.A., Surlyk, F., Piasecki, S., 2002. Terrestrial and marine extinction at the Triassic-Jurassic boundary synchronized with major carbon-cycle perturbation: a link to initiation of massive volcanism? Geology 30, 251–254. https://doi.org/10.1130/0091-7613(2002)030<0251:TAMEAT>2.0.CO;2.

Hillebrandt, A.v., Krystyn, L., Kürschner, W.M., Bonis, N.R., Ruhl, M., Richoz, S., Schobben, M.A.N., Urlichs, M., Bown, P.R., Kment, K., McRoberts, C.A., Simms, M., Tomãsových, A., 2013. The Global Stratotype Sections and Point (GSSP) for the base of the Jurassic System at Kuhjoch (Karwendel Mountains, Northern Calcareous Alps, Tyrol, Austria). Episodes 36, 162–198.

Jaffey, A.H., Flynn, K.F., Glendenin, L.E., Bentley, W.C., Essling, A.M., 1971. Precision measurement of half-lives and specific activities of ^{235}U and ^{238}U. Phys. Rev. C 4 (5), 1889–1906.

Kent, D.V., Olsen, P.E., Muttoni, G., 2017. Astrochronostratigraphic polarity time scale (APTS) for the Late Triassic and Early Jurassic from continental sediments and correlation with standard marine stages. Earth-Sci. Rev. 166, 153–180. https://doi.org/10.1016/j.earscirev.2016.12.014.

Kocsis, Á.T., Kiessling, W., Pálfy, J., 2014. Radiolarian biodiversity dynamics through the Triassic and Jurassic: implications for proximate causes of the end-Triassic mass extinction. Paleobiology 40 (4), 625–639.

Korte, C., Ruhl, M., Pálfy, J., Ullmann, C.V., Hesselbo, S.P., 2019. Chemostratigraphy across the Triassic–Jurassic boundary. In: Sial, A.N., Gaucher, C., Ramkumar, M., Ferreira, V.P. (Eds.), Chemostratigraphy Across Major Chronological Boundariess. In: Geophysical Monograph, vol. 240. American Geophysical Union (AGU), pp. 183–210.

Kovács, E.B., Ruhl, M., Demény, A., Fórizs, I., Hegyi, I., Horváth-Kostka, Z.R., Móricz, F., Vallner, Z., Pálfy, J., 2020. Mercury anomalies and carbon isotope excursions in the western Tethyan Csővár section support the link between CAMP volcanism and the end-Triassic extinction. Glob. Planet. Change, 103291.

Krystyn, L., 2010. Decision report on the defining event for the base of the Rhaetian stage. Albertiana 38, 11–12. http://paleo.cortland.edu/Albertiana/issues/Albertiana_38.

Krystyn, L., Bouquerel, H., Kürschner, W.M., Richoz, S., Gallet, Y., 2007. Proposal for a candidate GSSP for the base of the Rhaetian stage. In: Lucas, S.G., Spielmann, J.A. (Eds.), The Global Triassic. New Mexico Museum of Natural History and Science Bulletin, pp. 189–199.

Larina, E., Bottjer, D.J., Corsetti, F.A., Zonneveld, J.P., Celestian, A.J., Bailey, J.V., 2019. Uppermost Triassic phosphorites from Williston Lake, Canada: link to fluctuating euxinic-anoxic conditions in northeastern Panthalassa before the end-Triassic mass extinction. Sci. Rep. 9, 18790. https://doi.org/10.1038/s41598-019-55162-2.

Li, M., Zhang, Y., Huang, C., Ogg, J., Hinnov, L., Wang, Y., Zou, Z., Li, L., 2017. Astronomical tuning and magnetostratigraphy of the Upper Triassic Xujiahe Formation of South China and Newark Supergroup of North America: implications for the Late Triassic time scale. Earth Planet. Sci. Lett. 475, 207–223. https://doi.org/10.1016/j.epsl.2017.07.015.

Lindström, S., van de Schootbrugge, B., Hansen, K.H., Pedersen, G.K., Alsen, P., Thibault, N., Dybkjær, K., Bjerrum, C.J., Nielsen, L.H., 2017. A new correlation of Triassic–Jurassic boundary successions in NW Europe, Nevada and Peru, and the Central Atlantic Magmatic Province: a time-line for the end-Triassic mass extinction. Palaeogeogr. Palaeoclimatol. Palaeoecol. 478, 80–102. https://doi.org/10.1016/J.PALAEO.2016.12.025.

Longridge, L.M., Carter, E.S., Smith, P.L., Tipper, H.W., 2007. Early Hettangian ammonites and radiolarians from the Queen Charlotte Islands, British Columbia and their bearing on the definition of the Triassic-Jurassic boundary. Palaeogeogr. Palaeoclimatol. Palaeoecol. 244, 142–169.

Longridge, L.M., Pálfy, J., Smith, P.L., Tipper, H.W., 2008. Middle and late Hettangian (Early Jurassic) ammonites from the Queen Charlotte Islands, British Columbia, Canada. Rev. Paléobiol. 27 (1), 191–248.

Maron, M., Rigo, M., Bertinelli, A., Katz, M.E., Godfrey, L., Zaffani, M., Muttoni, G., 2015. Magnetostratigraphy, biostratigraphy, and chemostratigraphy of the Pignola–Abriola section: new constraints for the Norian–Rhaetian boundary. Geol. Soc. Am. Bull. 127, 962–974. https://doi.org/10.1130/b31106.1.

Maron, M., Muttoni, G., Rigo, M., Gianolla, P., Kent, D., 2019. New magneto-biostratigraphic results from the Ladinian of the Dolomites and implications for the Triassic geomagnetic polarity timescale. Palaeogeogr. Palaeoclimatol. Palaeoecol. 517, 52–73.

McElwain, J.C., Beerling, D.J., Woodward, F.I., 1999. Fossil plants and global warming at the Triassic-Jurassic boundary. Science 285 (5432), 1386–1390. https://doi.org/10.1126/science.285.5432.1386.

McRoberts, C.A., Ward, P.D., Hesselbo, S., 2007. A proposal for the base Hettangian Stage (=base Jurassic System) GSSP at New York Canyon (Nevada, USA) using carbon isotopes. ISJS Newsletter 34 (1), 43–49.

Muttoni, G., Kent, D.V., Jadoul, F., Olsen, P.E., Rigo, M., Galli, M.T., Nicora, A., 2010. Rhaetian magneto-biostratigraphy from the southern Alps (Italy): constraints on Triassic chronology. Palaeogeogr. Palaeoclimatol. Palaeoecol. 285, 1–16. https://doi.org/10.1016/j.palaeo.2009.10.014.

Pálfy, J., Kocsis, Á.T., 2014. Volcanism of the Central Atlantic magmatic province as the trigger of environmental and biotic changes around the Triassic- Jurassic boundary. In: Keller, G., Kerr, A.C. (Eds.), Volcanism, Impacts, and Mass Extinctions: Causes and Effects. In: Geol. Soc. Am., Spec. Pap., vol. 505, pp. 245–261.

Pálfy, J., Mortensen, J.K., Carter, E.S., Smith, P.L., Friedman, R.M., Tipper, H.W., 2000. Timing the end-Triassic mass extinction: first on land, then in the sea? Geology 28, 39. https://doi.org/10.1130/0091-7613(2000)28<39:TTEMEF>2.0.CO;2.

Pálfy, J., Demény, A., Haas, J., Carter, E.S., Görög, Á., Halász, D., Zajzon, N., 2007. Triassic-Jurassic boundary events inferred from integrated stratigraphy of the Csővár section, Hungary. Palaeogeogr. Palaeoclimatol. Palaeoecol. 244 (1–4), 11–33. https://doi.org/10.1016/j.palaeo.2006.06.021.

Palotai, M., Pálfy, J., Sasvári, Á., 2017. Structural complexity at and around the Triassic–Jurassic GSSP at Kuhjoch, Northern Calcareous Alps, Austria. Int. J. Earth Sci. 106 (7), 2475–2487.

Pieńkowski, G., Hesselbo, S.P., Barbacka, M., Leng, M.J., 2020. Non-marine carbon-isotope stratigraphy of the Triassic-Jurassic transition in the Polish Basin and its relationships to organic carbon preservation, pCO2 and palaeotemperature. Earth-Science Reviews 210, 103383. https://doi.org/10.1016/j.earscirev.2020.103383.

Rigo, M., Bertinelli, A., Concheri, G., Gattolin, G., Godfrey, L., Katz, M.E., Maron, M., Mietto, P., Muttoni, G., Sprovieri, M., Stellin, F., Zaffani, M., 2016. The Pignola-Abriola section (southern Apennines, Italy): a new GSSP candidate for the base of the Rhaetian Stage. Lethaia 49 (3), 287–306. https://doi.org/10.1111/let.12145.

Rigo, M., Mazza, M., Karádi, V., Nicora, A., 2018. New Upper Triassic conodont biozonation of the Tethyan Realm. In: Tanner, L.H. (Ed.), The Late Triassic World: Earth in a Time of Transition. In: Top. Geobiol., vol. 46, pp. 189–235.

Rigo, M., Onoue, T., Tanner, L., Lucas, S.G., Godfrey, L., Katz, M.E., Zaffani, M., Grice, K., Cesar, J., Yamashita, D., Maron, M.M., Tackett, L.S., Campbell, H., Tateo, F., Concheri, G., Agnini, C., Chiari, M., Bertinelli, A., 2020. The Late Triassic Extinction at the Norian/Rhaetian boundary: biotic evidence and geochemical signature. Earth-Sci. Rev. 204, 103180. https://doi.org/10.1016/j.earscirev.2020.103180.

Ruhl, M., Kürschner, W.M., Krystyn, L., 2009. Triassic–Jurassic organic carbon isotope stratigraphy of key sections in the western Tethys realm (Austria). Earth Planet. Sci. Lett. 281 (3–4), 169–187.

Ruhl, M., Kürschner, W.M., 2011. Multiple phases of carbon cycle disturbance from large igneous province formation at the Triassic-Jurassic transition. Geology 39, 431–434. https://doi.org/10.1130/G31680.1.

Ruhl, M., Hesselbo, S.P., Al-Suwaidi, A., Jenkyns, H.C., Damborenea, S.E., Manceñido, M.O., Storm, M., Mather, T.A., Riccardi, A.C., 2020. On the onset of Central Atlantic Magmatic Province (CAMP) volcanism and environmental and carbon-cycle change at the Triassic-Jurassic transition (Neuquén Basin, Argentina). Earth-Sci. Rev. 208, 103229. https://doi.org/10.1016/j.earscirev.2020.103229.

Schaller, M.F., Wright, J.D., Kent, D.V., 2011. Atmospheric PCO_2 perturbations associated with the Central Atlantic Magmatic Province. Science 331, 1404–1409. https://doi.org/10.1126/science.1199011.

Schoene, B., Guex, J., Bartolini, A., Schaltegger, U., Blackburn, T.J., 2010. Correlating the end-Triassic mass extinction and flood basalt volcanism at the 100 ka level. Geology 38, 387–390. https://doi.org/10.1130/G30683.1.

Senowbari-Daryan, B., Link, M., 2019. *Heterastridium* (Hydrozoa) from the Norian of Iran and Turkey. Palaeontogr. A: Palaeozool. – Stratigr. 314 (4–6), 81–159.

Stamatakos, J.A., Trop, J.M., Ridgway, K.D., 2001. Late Cretaceous paleogeography of Wrangellia: Paleomagnetism of the MacColl Ridge Formation, southern Alaska, revisited. Geology 29 (10), 947–950. https://doi.org/10.1130/0091-7613(2001)029<0947:LCPOWP>2.0.CO;2.

Steinthorsdottir, M., Jeram, A.J., McElwain, J.C., 2011. Extremely elevated CO_2 concentrations at the Triassic/Jurassic boundary. Palaeogeogr. Palaeoclimatol. Palaeoecol. 308 (3–4), 418–432. https://doi.org/10.1016/j.palaeo.2011.05.050.

Tanner, L.H., Lucas, S.G., 2015. The Triassic-Jurassic strata of the Newark Basin, USA: a complete and accurate astronomically-tuned timescale? Stratigraphy 12, 47–65.

Taylor, D.G., Guex, J., Rakús, M., 2001. Hettangian and Sinemurian ammonoid zonation for the western Cordillera of North America. Bull. Soc. Vaud. Sci. Nat. 87, 381–421.

Tozer, E.T., 1994. Canadian Triassic ammonoid faunas. Bull., Geol. Surv. Can. 467. 663 p.

Trop, J.M., Benowitz, J.A., Koepp, D.Q., Sunderlin, D., Brueseke, M.E., Layer, P.W., Fitzgerald, P.G., 2020. Stitch in the ditch: Nutzotin Mountains (Alaska) fluvial strata and a dike record ca. 117–114 Ma accretion of Wrangellia with western North America and initiation of the Totschunda fault. Geosphere 16 (1), 82–110.

Ward, P.D., Haggart, J.W., Carter, E.S., Wilbur, D., Tipper, H.W., Evans, T., 2001. Sudden productivity collapse associated with the Triassic-Jurassic boundary mass extinction. Science 292, 1148–1151. https://doi.org/10.1126/science.1058574.

Whiteside, J.H., Olsen, P.E., Eglinton, T.I., Brookfield, M.E., Sambrotto, R.N., 2010. Compound-specific carbon isotopes from Earth's largest flood basalt eruptions directly linked to the end-Triassic mass extinction. Proc. Natl. Acad. Sci. 107, 6721–6725. https://doi.org/10.1073/pnas.1001706107.

Wignall, P.B., 2001. Large igneous provinces and mass extinctions. Earth-Sci. Rev. 53, 1–33. https://doi.org/10.1016/S0012-8252(00)00037-4.

Williford, K.H., Grice, K., Holman, A., McElwain, J.C., 2014. An organic record of terrestrial ecosystem collapse and recovery at the Triassic-Jurassic boundary in East Greenland. Geochim. Cosmochim. Acta 127, 251–263. https://doi.org/10.1016/j.gca.2013.11.033.

Witmer, J.W., 2007. Sedimentology and stratigraphy of the Upper Triassic - lower Jurassic McCarthy formation, Wrangell Mountains, South-Central Alaska. Unpublished BSc Thesis. Bucknell University.

Wotzlaw, J.F., Guex, J., Bartolini, A., Gallet, Y., Krystyn, L., McRoberts, C.A., Taylor, D., Schoene, B., Schaltegger, U., 2014. Towards accurate numerical calibration of the Late Triassic: high-precision U–Pb geochronology constraints on the duration of the Rhaetian. Geology 42, 571–574. https://doi.org/10.1130/g35612.1.